JOURNAL OF MATERIALS SCIENCE **40** (2005) 6151–6156

Dielectric characteristics of $Pb(Zn_{1/3}Ta_{2/3})O_3$-$BaTiO_3$ ceramics with/without $PbTiO_3$ modification

KYUNG-HAN SEO, BONG-HO LEE, NAM-KYOUNG KIM
Department of Inorganic Materials Engineering, Kyungpook National University, Daegu, 702-701, Korea

JAEJUNG KO
Department of Chemistry, Korea University, Chochiwon, Chungnam 339-700, Korea

Published online: 8 September 2005

Stabilization tendencies of the perovskite structure in a $Pb(Zn_{1/3}Ta_{2/3})O_3$-$BaTiO_3$ pseudobinary system with/without compositional modification by 20 mol% $PbTiO_3$ introduction were compared. In order to promote perovskite phase formation, the B-site precursor method (which is conceptually similar to the columbite process) was employed in this study. Dielectric properties of sintered samples were investigated as functions of composition and measurement frequency. Dielectric constant spectra, in the paraelectric temperature region, were further analyzed in terms of diffuseness. Microstructures of sintered specimens were also investigated and correlated with perovskite stabilization.

1. Introduction

Lead zinc niobate $Pb(Zn_{1/3}Nb_{2/3})O_3$ and lead magnesium niobate $Pb(Mg_{1/3}Nb_{2/3})O_3$ (abbreviated as PZN and PMN, respectively), are complex-perovskite relaxor compounds [1–3]. By contrast, lead zinc tantalate $Pb(Zn_{1/3}Ta_{2/3})O_3$ (PZT) has not been yet synthesized to a perovskite structure [4–9], despite the perovskite stoichiometry identical to PZN/PMN. It should be noted that PZT in the present paper does not stand for the well-known $Pb(Zr,Ti)O_3$, but for the tantalum analog of PZN.

So far, many attempts have been conducted on the stabilization of perovskite PZN via compositional modifications by $BaTiO_3$ [10–13], $PbTiO_3$ [4, 10, 13–15], $BaZrO_3$ [11], $PbZrO_3$ [11], $Ba(Zn_{1/3}Nb_{2/3})O_3$ [12, 16], PMN [17], and $Pb(Mg_{1/3}Ta_{2/3})O_3$ (PMT) [18]. For PZT, however, only a few cases have been reported by $Ba(Zn_{1/3}Ta_{2/3})O_3$ [6], $PbTiO_3$ [9, 19, 20], PMN [8], and PMT [7] additions. Such attempts, however, resulted in only marginal success.

In the present study, therefore, simultaneous additions of $BaTiO_3$ and/or $PbTiO_3$ were attempted and the consequent results are compared. Stability of the perovskite structure and the consequent dielectric properties of the ceramics were examined. Since the presence of the parasitic pyrochlore (even in small quantities) has been reported to be detrimental to dielectric properties [4, 21, 22], a B-site precursor method [23, 24] was employed in the powder preparation in order to stabilize the perovskite structure. In this method, the (B′, B″) O_2-type precursors were synthesized separately and later reacted with the A-site components to form the A(B′, B″) O_3 perovskite. The B-site precursor method, which is conceptually similar to the columbite process [25, 26] but rather comprehensive, has been proven to be highly effective in perovskite synthesis, especially for pyrochlore-prone compositions.

2. Experimental

Nominal compositions of the two systems (Fig. 1) can be formulated as $(1-x)Pb(Zn_{1/3}Ta_{2/3})O_3$-$xBaTiO_3$ and $(0.8-y)Pb(Zn_{1/3}Ta_{2/3})O_3$-$yBaTiO_3$-$0.2PbTiO_3$, i.e., $(Pb_{1-x}Ba_x)[(Zn_{1/3}Ta_{2/3})_{1-x}Ti_x]O_3$ and $(Pb_{1-y}Ba_y)[(Zn_{1/3}Ta_{2/3})_{0.8-y}Ti_{0.2+y}]O_3$ (or $(1-x)$PZT-xBT and $(0.8-y)$PZT-yBT-0.2PT, respectively). The two systems will be designated hereinafter as Systems I and II. Source materials used were high-purity oxide and carbonate chemicals of PbO (99.5%), $BaCO_3$ (99.9%), ZnO (99.8%), Ta_2O_5 (99.9%), and TiO_2 (99.9%).

The overall experimental procedures are schematically presented in Fig. 2. B-site precursor powders of the two systems were prepared with respect to the formulations of $[(Zn_{1/3}Ta_{2/3})_{1-x}Ti_x]O_2$ and $[(Zn_{1/3}Ta_{2/3})_{0.8-y}Ti_{0.2+y}]O_2$, with a relation of $x = 0.2 + y$. Hence, the precursor compositions of $y = 0.0$ to 0.8 (System II) are identical to those of $x = 0.2$ to 1.0 (System I). Mixed powders were milled for 12 h in ethanol, using ZrO_2 balls in polyethylene bottles. Milled batches were dried for 24 h and calcined at 1200–1250°C for 2 h in a covered alumina crucible. The calcination procedures were repeated one more

0022-2461
DOI: 10.1007/s10853-005-3164-4

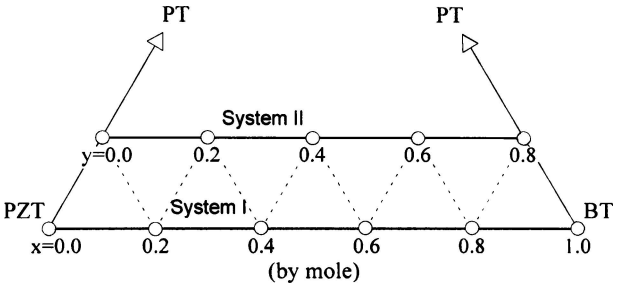

Figure 1 Investigated compositions in Systems I and II.

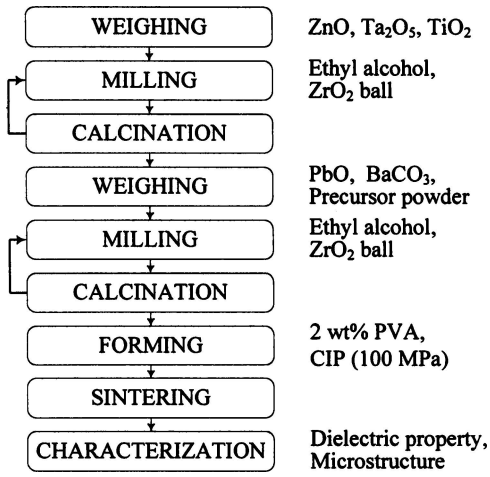

Figure 2 Flow diagram of the experimental procedure.

time for each composition. After the addition of PbO and $BaCO_3$ in stoichiometric ratios (i.e., without the addition of any excess amount), the powder mixtures of the two systems were milled, dried, and calcined first at 800–850°C for 2 h and then at 900–1000°C for 2 h, with intermediate milling-to-drying steps. Developed phases of the resulting powders were determined by X-ray diffraction (XRD) using CuKα radiation.

Prepared powders (with 2 wt% polyvinyl alcohol added as a binder) were uniaxially formed into pellets (~10 mmϕ and ~1 mm thick) and further compacted by cold-isostatic pressing (CIP) at 100 MPa. The preforms were densified in a multiple-enclosure inverted-crucible setup [18], filled with powders of the same composition. Optimum sintering temperatures were found to be 1200–1350°C and 1100–1300°C (soaking time = 1 h) for Systems I and II, respectively. In each system, the temperatures increased gradually with increasing fractions of BT. Gold was sputtered onto the sintered samples as electrical contacts for dielectric characterization. Dielectric constant values in the samples were measured during the cooling cycle using an impedance analyzer under weak-field (~1 V/mm_{rms}) and low-frequency (10^3–10^6 Hz) conditions. Gold-coated fracture surfaces were examined by a scanning electron microscope (SEM).

3. Results and discussion

XRD patterns of the B-site precursor compositions are shown in Fig. 3. At $x = 0.0$ of $(Zn_{1/3}Ta_{2/3})O_2$, only the diffraction peaks of a tri-αPbO_2 structure ($ZnTa_2O_6$, ICDD No. 39-1484) were observed. The compositions

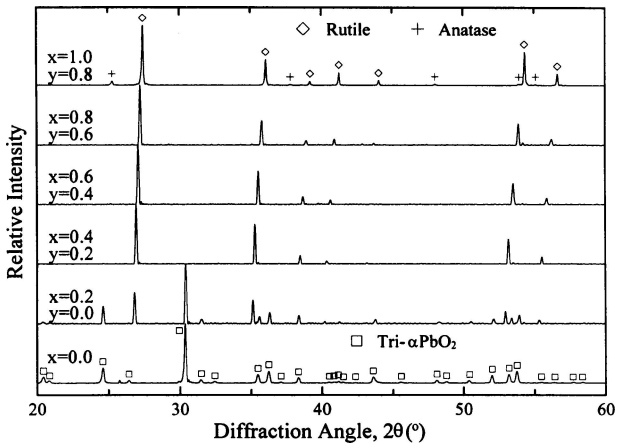

Figure 3 X-ray diffraction patterns of the two B-site precursor systems of $[(Zn_{1/3}Ta_{2/3})_{1-x}Ti_x]O_2$ and $[(Zn_{1/3}Ta_{2/3})_{0.8-y}Ti_{0.2+y}]O_2$.

of $x = 0.2$ to 0.8 (i.e., $y = 0.0$ to 0.6) can be expressed as

$$x = 0.2, \quad y = 0.0 : [(Zn_{1/3}Ta_{2/3})_{0.8}Ti_{0.2}]O_2 = 0.6(Zn_{1/3}Ta_{2/3})O_2 + 0.4[(Zn_{1/3}Ta_{2/3})_{1/2}Ti_{1/2}]O_2, \quad (1)$$

$$x = 0.4, \quad y = 0.2 : [(Zn_{1/3}Ta_{2/3})_{0.6}Ti_{0.4}]O_2 = 0.2(Zn_{1/3}Ta_{2/3})O_2 + 0.8[(Zn_{1/3}Ta_{2/3})_{1/2}Ti_{1/2}]O_2, \quad (2)$$

$$x = 0.6, \quad y = 0.4 : [(Zn_{1/3}Ta_{2/3})_{0.4}Ti_{0.6}]O_2 = 0.8[(Zn_{1/3}Ta_{2/3})_{1/2}Ti_{1/2}]O_2 + 0.2TiO_2, \quad (3)$$

$$x = 0.8, \quad y = 0.6 : [(Zn_{1/3}Ta_{2/3})_{0.2}Ti_{0.8}]O_2 = 0.4[(Zn_{1/3}Ta_{2/3})_{1/2}Ti_{1/2}]O_2 + 0.6TiO_2. \quad (4)$$

At $x = 0.2$ (i.e., $y = 0.0$), two structures of tri-αPbO_2 $(Zn_{1/3}Ta_{2/3})O_2$ and rutile $[(Zn_{1/3}Ta_{2/3})_{1/2}Ti_{1/2}]O_2$ (ICDD No. 39-292) were identified with somewhat higher intensity levels of the former, which are well consistent with Equation (1). Similarly, coexistence of the two structures at $x = 0.4$ (i.e., $y = 0.2$) was also predictable by the compositional resolution of Equation (2). In the XRD results, however, only the rutile structure was detected, from which it can be deduced that the $(Zn_{1/3}Ta_{2/3})O_2$ component (20 mol% fraction) had dissolved completely into the rutile solid solution.

For $x = 0.6$ and 0.8 (i.e., $y = 0.4$ and 0.6, respectively), compositional partitioning into $[(Zn_{1/3}Ta_{2/3})_{1/2}Ti_{1/2}]O_2$ and TiO_2 (rutile structure, ICDD No. 21-1276) was predicted in Equations 3 and 4. The two components are isostructural, whose cationic radii [27] are 0.0639 nm (weight-averaged value) and 0.0605 nm, respectively. These values are well within the Hume-Rothery tolerance range. Therefore, it can be expected that the two components (molar ratios of 8:2 and 4:6, respectively) would readily form solid solutions. In the X-ray profiles, only a monophasic rutile structure was actually identified, thus confirming complete formation of the solid solution. Finally at $x = 1.0$ (i.e., $y = 0.8$, TiO_2), a typical diffraction profile of the rutile structure was observed. Moreover, minor

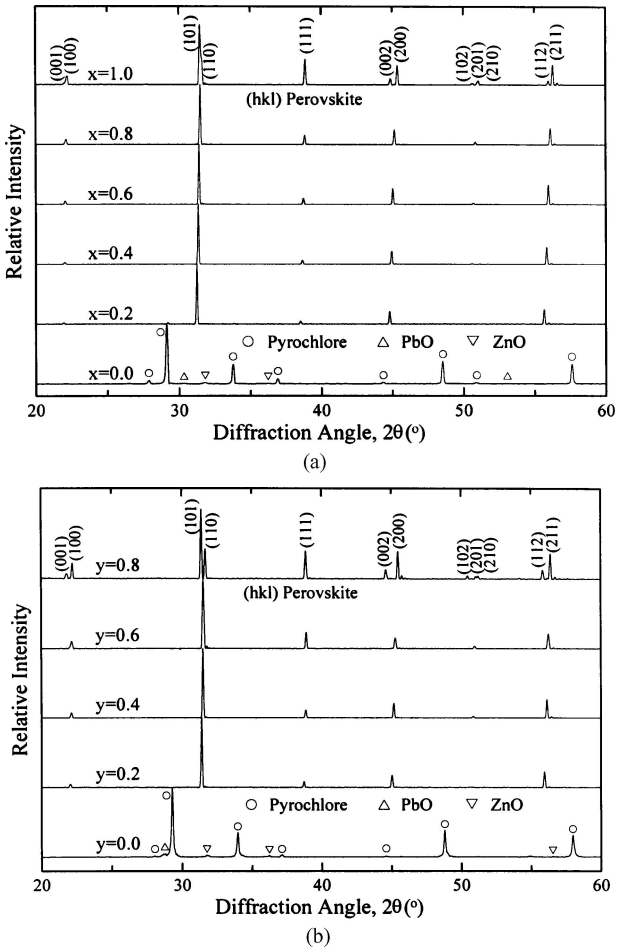

Figure 4 X-ray diffraction patterns of the (a) $(1-x)Pb(Zn_{1/3}Ta_{2/3})O_3$-$xBaTiO_3$ (System I) and (b) $(0.8-y)Pb(Zn_{1/3}Ta_{2/3})O_3$-$yBaTiO_3$-$0.2PbTiO_3$ (System II).

peaks of the parasitic anatase structure (ICDD No. 21-1272) were additionally detected, which undoubtedly resulted from the raw chemical of TiO_2. Throughout the whole compositions, however, diffraction angles of the rutile solid solution increased substantially with increasing values of x and y. The steady shifts can be explained easily by the gradual replacement of $Zn_{1/3}Ta_{2/3}$ (0.0673 nm, weight-averaged value [27]) by the smaller Ti (0.0605 nm [27]).

XRD results of Systems I and II are compared in Figs 4a and b. At $x = 0.0$ (PZT) and $y = 0.0$ (0.8PZT-0.2PT), only a cubic pyrochlore structure was identified along with negligible amounts of PbO and ZnO. The two oxide components are believed to be the by-products, left after the pyrochlore formation from the powder mixtures of perovskite stoichiometry [28]. At $x = 0.2$ (0.8PZT-0.2BT), most of the pyrochlore peaks were replaced by those of a (pseudo)cubic perovskite structure, leaving only a negligible fraction of pyrochlore (2.2%, estimated by intensity comparison between those of the pyrochlore and perovskite as $I_{pyro.}/(I_{pyro} + I_{perov.})$). When the X-ray results of $x = 0.2$ and $y = 0.0$ are compared, BT turned out to be much more efficient than PT in terms of perovskite stabilization, as previously reported [4]. At higher values of x and y (i.e., BT fractions) in the two systems, only the perovskite structure was detected without any trace of pyrochlore. Hence, the perovskite contents were 100%

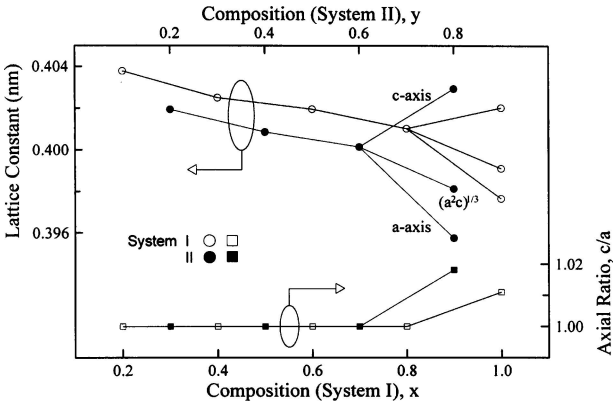

Figure 5 Lattice parameters of the perovskite structure in Systems I and II.

at $0.4 \leq x$ and $0.2 \leq y$. Meanwhile, splittings into several peaks were observed at $x = 1.0$ (System I) and $y = 0.8$ (System II), indicating the development of tetragonal symmetry. Relative densities of the sintered ceramics of the two systems were 94–98% and 95–98% of their respective theoretical values. The samples of $x = 0.0$, however, could not be properly sintered for further characterization. As a result, the composition can not be subject to further investigation.

Lattice parameters of the perovskite structure, estimated from the XRD data (Fig. 4) by using Cohen's method (assuming (pseudo)cubic and tetragonal symmetries), are contrasted in Fig. 5. The parameters decreased rather linearly with increasing BT fractions in both systems, indicating gradual contraction of the unit cell dimensions, which is a result of the Ti replacement for $Zn_{1/3}Ta_{2/3}$. Moreover, the decreasing rates were very similar, regardless of the $PbTiO_3$ component incorporated in System II. As discussed, tetragonal symmetries developed at high fractions of BT (Fig. 4), leading to the axial ratios of $c/a = 1.011$ ($x = 1.0$, BT) and 1.018 ($y = 0.8$, 0.8BT-0.2PT). The higher ratio at $y = 0.8$ can be easily explained by the higher value of PT ($c/a = 1.065$, ICDD No. 6-452).

Contrasting dielectric constant spectra of the representative compositions ($x = 0.4$, 1.0 and $y = 0.2$, 0.8 in Systems I and II) are compared as a function of frequency as shown in Fig. 6. Magnitudes of the maximum

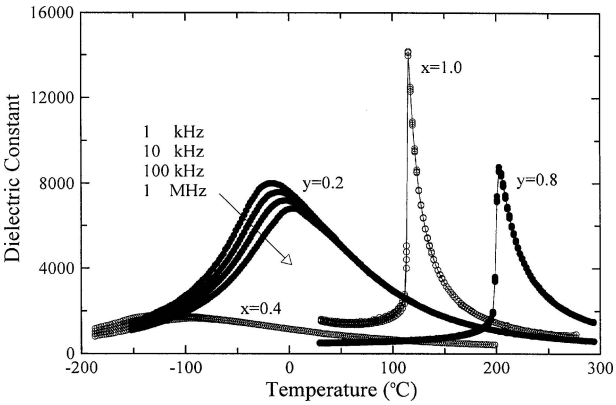

Figure 6 Dependence of the dielectric constant spectra upon measurement frequency for $x = 0.4$ and 1.0 (System I), and $y = 0.2$ and 0.8 (System II).

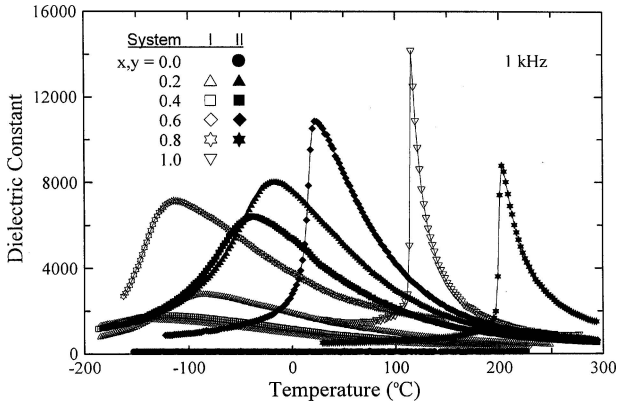

Figure 7 Dielectric constant spectra of Systems I and II (@1 kHz).

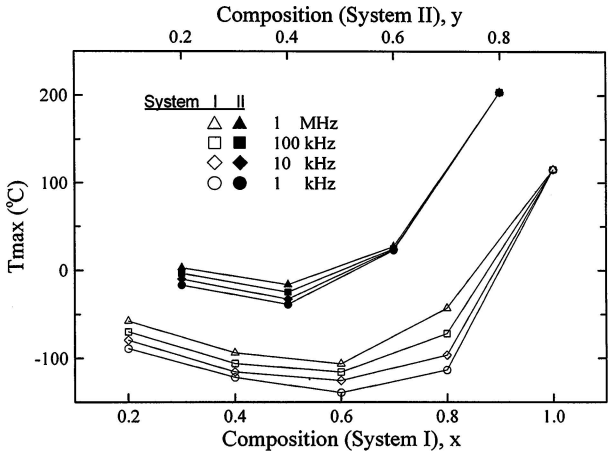

Figure 8 Frequency-dependent T_{max} values of Systems I and II.

dielectric constant (K_{max}) and corresponding temperatures (T_{max}) of $y = 0.2$ were determined to be 8000 (−17°C), 7580 (−10°C), 7190 (−3°C), and 6810 (3°C) at 1, 10, 100, and 1000 kHz, respectively, whereas those of $x = 0.4$ were only 1810 (−122°C), 1750 (−116°C), 1710 (−106°C), and 1640 (−94°C) at the same frequency decades. Nevertheless, frequency-dependent dielectric dispersion of decreasing K_{max} and increasing T_{max} with increasing measurement frequency was well demonstrated in both compositions. By contrast, normal ferroelectric behavior (little dependence of K_{max} and T_{max} upon measurement frequency) was observed at $x = 1.0$ and $y = 0.8$. The respective values were 14,200, 14,150, 14,100, and 14,000 (115°C, $x = 1.0$) and 8860, 8720, 8670, and 8660 (203°C, $y = 0.8$). Meanwhile, phase transition modes in the former compositions ($x = 0.4$ and $y = 0.2$) were very diffuse, whereas the modes were quite sharp in the latter two ($x = 1.0$ and $y = 0.8$).

Dielectric constant spectra (@1 kHz) of the entire compositions in Systems I and II are contrasted in Fig. 7. The spectrum of $y = 0.0$ did not exhibit any dielectric constant peaks in the measured temperature range, but merely decreased at a rate of 730 ppm/K with a room-temperature value of ~84. Meanwhile, the K_{max} values of the two systems did not vary linearly with the compositional changes. Instead, the values were the lowest at $x = 0.6$ and $y = 0.4$, 1640 (−140°C) and 6420 (−38°C), respectively. By contrast, the values were as high as 14,200 (115°C, $x = 1.0$) and 10,900 (23°C, $y = 0.6$).

Variations of T_{max} in Systems I and II are plotted in Fig. 8 against composition and measurement frequency. The temperatures (@1 kHz) of the two systems varied from −86°C ($x = 0.2$) to 115°C ($x = 1.0$) and from −17°C ($y = 0.2$) to 203°C ($y = 0.8$). The values, however, were also the lowest at intermediate compositions in both systems, −140°C ($x = 0.6$) and −38°C ($y = 0.4$). In addition, the temperatures of System II were consistently higher than those of System I. This is obviously due to the incorporation of 20 mol% PT with a dielectric constant peak at 490°.

Dielectric constant spectra of the two systems in the paraelectric temperature region were further analyzed to investigate the diffuseness characteristics. A detailed physical meaning and the derivation method of

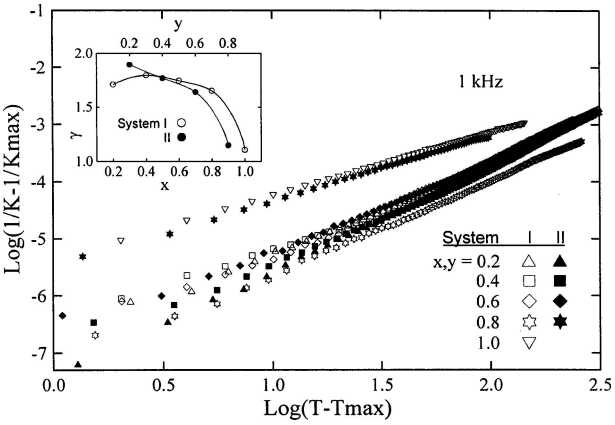

Figure 9 Log(1/K − 1/K_{max}) versus log(T − T_{max}) relations for the compositions in Systems I and II. Variations of γ are included in the inset.

the diffuseness exponent (γ) can be found elsewhere [16, 29–31]. Required plots of log(1/K-1/K_{max}) versus log(T-T_{max}) for the compositions in Systems I and II are presented in Fig. 9. The γ values were determined from the slopes of the log-log relation and the results are shown in the inset of Fig. 9. The high values of γ (1.80 and 1.89 at $x = 0.4$ and $y = 0.2$, respectively) decreased slowly to medium values of x and y, followed by quite steep decline to 1.10 ($x = 1.0$) and 1.15 ($y = 0.8$).

Fractal surface observations were carried out using SEM as shown in Fig. 10. Only small-sized grains were present at $y = 0.0$, where the perovskite phase ratio was 0%. Hence, the small grains are obviously those of the pyrochlore phase. A similar microstructure has been frequently observed in other pyrochlore-prone compositions. At $x = 0.2$ (perovskite phase ratio = 97.8%), large grains were mostly observed, along with small ones dispersed at grain boundaries and junctions. At $y = 0.4$ and $x = 0.6$ (perovskite phase ratios = 100%), typical micrographs of multi-faceted perovskite grains were obtained. Moreover, the fracture modes were entirely transgranular, as reported in many lead-containing complex-perovskite ceramics. Other compositions of the two systems (where the perovskite phase ratios were 100%) also showed similar microstructures with average grain sizes in the range of 2–4 μm.

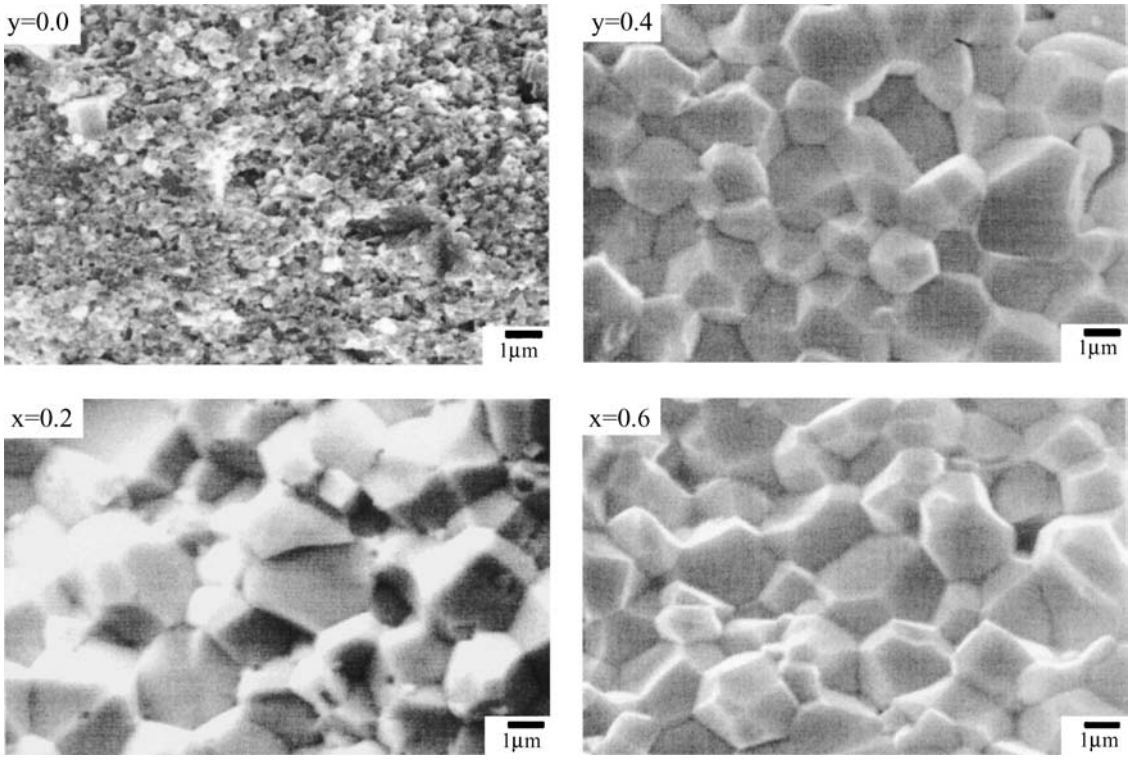

Figure 10 Fracture-surface microstructures of $x = 0.2$ and 0.6 (System I), and $y = 0.0$ and 0.4 (System II).

4. Summary

In the B-site precursor compositions of the two systems, a rutile structure was observed at $0.2 \leq x$ (i.e., $0.0 \leq y$), along with a coexisting trirutile structure at $x = 0.0$ and $x = 0.2$ ($y = 0.0$). After the addition of PbO and $BaCO_3$ with proper calcination, the perovskite formation was complete in the entire investigated compositions, except for the perovskite contents of 0% ($x = 0.0$ and $y = 0.0$ of PZT and 0.8PZT-0.2PT, respectively) and 97.8% ($x = 0.2$, i.e., 0.8PZT-0.2BT). Compared with PT, therefore, BT was found to be much more effective in the stabilization of the perovskite structure. With increasing values of x and y in the two systems, tetragonal symmetries of the perovskite structure started to develop at high BT fractions of $0.8 < x$ and $0.6 < y$.

Dielectric constant spectra of the PZT-rich compositions (low values of x and y) exhibited frequency-dependent relaxation in general, whereas those of the BT-rich compositions did not show such behavior. In addition, the dielectric spectra of $x \leq 0.8$ (System I) and of $y = 0.2$ and 0.4 (System II) were rather diffuse, regardless of measurement frequency. By contrast, those of the remaining compositions were quite sharp, except for the spectra of $y = 0.0$, which did not show any dielectric maximum peaks. Temperatures of the dielectric constant peaks were the lowest at intermediate compositions in both systems. Magnitudes of the diffuseness exponent (γ) were rather insensitive to the compositional change at low-to-medium values of x and y.

Acknowledgment

This study was supported by a grant from the Korea Science and Engineering Foundation (KOSEF) through the Basic Research Program (R05-2003-000-10068-0).

References

1. G. A. SMOLENSKII, *J. Phys. Soc. Jpn.* **28** (Suppl). (1970) 26.
2. L. E. CROSS, *Ferroelectrics* **76** (1987) 241.
3. *Idem.*, *ibid.* **151** (1994) 305.
4. T. R. SHROUT and A. HALLIYAL, *Am. Ceram. Soc. Bull.* **66** (1987) 704.
5. H. C. LING, M. F. YAN and W. W. RHODES, *Ferroelectrics* **89** (1989) 69.
6. B.-Y. AHN and N.-K. KIM, *Mater. Res. Bull.* **35** (2000) 1677.
7. S.-M. LIM and N.-K. KIM, *J. Mater. Sci.* **35** (2000) 4373.
8. M.-C. CHAE, S.-M. LIM and KIM, KIM, *Ferroelectrics* **242** (2000) 25.
9. J.-S. KIM, N.-K. KIM and H. KIM, *J. Am. Ceram. Soc.* **86** (2003) 929.
10. A. HALLIYAL, U. KUMAR, R. E. NEWNHAM and L. E. CROSS, *ibid.* **70** (1987) 119.
11. *Idem.*, *Am. Ceram. Soc. Bull.* **66** (1987) 671.
12. J.-K. LEE, S.-G. KANG and H. KIM, *J. Mater. Sci.* **33** (1998) 693.
13. W. Z. ZHU, A. KHOLKIN, P. Q. MANTAS and J. L. BAPTISTA, *ibid.* **36** (2001) 3447.
14. J. KUWATA, K. UCHINO and S. NOMURA, *Ferroelectrics* **37** (1981) 579.
15. T. R. GURURAJA, A. SAFARI and A. HALLIYAL, *Am. Ceram. Soc. Bull.* **65** (1986) 1601.
16. B.-Y. AHN and N.-K. KIM, *J. Am. Ceram. Soc.* **83** (2000) 1720.
17. M.-C. CHAE, N.-K. KIM, J.-J. KIM and S.-H. CHO, *J. Mater. Sci.* **33** (1998) 1343.
18. *Idem.*, *Ferroelectrics*, **211** (1998) 25.
19. K. H. SEO, B. H. LEE and N. K. KIM, *Int. J. Modern Phys. B* **17** (2003) 1304.
20. K.-H. SEO and N.-K. KIM, submitted to *J. Mater. Sci.*
21. J. CHEN, A. GORTON, H. M. CHAN and M. P. HARMER, *J. Amer. Ceram. Soc.* **69** (1986) C303.

22. M. F. YAN, H. C. LING and W. W. RHODES, *J. Mater. Res.* **4** (1989) 930.
23. B.-H. LEE, N.-K. KIM, J.-J. KIM and S.-H. CHO, *Ferroelectrics* **211** (1998) 233.
24. S. ANANTA and N. W. THOMAS, *J. Eur. Ceram. Soc.* **19** (1999) 155.
25. S. L. SWARTZ and T. R. SHROUT, *Mater. Res. Bull.* **17** (1982) 1245.
26. S. L. SWARTZ, T. R. SHROUT, W. A. SCHULZE and L. E. CROSS, *J. Am. Ceram. Soc.* **67** (1984) 311.
27. R. D. SHANNON, *Acta Crystallogr.*, **A32** (1976) 751.
28. B.-Y. AHN and N.-K. KIM, *J. Mater. Sci.* **37** (2002) 4697.
29. K. UCHINO and S. NOMURA, *Ferroelectrics Lett.* **44** (1982) 55.
30. S. J. BUTCHER and N. W. THOMAS, *J. Phys. Chem. Solids* **52** (1991) 595.
31. M. KUWABARA, S. TAKAHASHI, K. GODA, K. OSHIMA and K. WATANABE, *Jpn. J. Appl. Phys.* **31** (1992) 3241.

Received 18 May 2004
and accepted 9 May 2005